Journal of The Electrochemical Society, **162** (8) F854-F867 (2015)
0013-4651/2015/162(8)/F854/14/$33.00 © The Electrochemical Society

Modeling and Experimental Validation of Pt Loading and Electrode Composition Effects in PEM Fuel Cells

Liang Hao,[a,*] Koji Moriyama,[b] Wenbin Gu,[c] and Chao-Yang Wang[a,d,*,z]

[a]*Electrochemical Engine Center (ECEC), and Department of Mechanical and Nuclear Engineering, The Pennsylvania State University, University Park, Pennsylvania 16802, USA*
[b]*Honda R&D Co. Ltd., Haga-machi, Haga-gun, Tochigi 321-3393, Japan*
[c]*General Motors, Pontiac, Michigan 48340, USA*
[d]*EC Power, State College, Pennsylvania 16803, USA*

A low platinum loading model, considering both the platinum loading and platinum particle distribution on carbon support, is developed. This model takes into account the interfacial transport resistances at ionomer, water film and Pt particle surfaces in order to capture the effects of Pt loading and electrode composition on fuel cell performance. After coupling this electrode model into a comprehensive PEM fuel cell model, i.e. M2 model, experimental validation is performed for a wide range of Pt loading from 0.2 to 0.025 mg/cm^2 for two electrode compositions with and without carbon dilution. Good agreement between the predicted and measured polarization curves is achieved under wide-ranging operating conditions. The agglomerate size effect is also examined and it is shown that the agglomerates have virtually no effect on cell performance for agglomerate radius smaller than 150 nm. Since in realistic fuel cell catalyst layers, agglomerates may not exist, or may only exist with sizes no larger than 150 nm based on SEM observations, the present work suggests that the standard homogeneous electrode model is suitable and sufficient for analyses of transport losses in PEM fuel cell electrodes where interfacial transport resistances exist.

Manuscript submitted April 2, 2015; revised manuscript received April 28, 2015. Published May 13, 2015.

Performance, durability, and especially cost are still the main challenges for commercialization of PEM fuel cell vehicles. Per the US Department of Energy (DOE) technical target, loading of the platinum group metal must be reduced to 0.125 mg/cm^2 or less in a fuel cell vehicle before 2017.[1] Although dramatic reduction of Pt loading has been achieved in the past decade, the current level of Pt loading still approaches or exceeds 0.25 mg/cm^2, which is twice the DOE short-term target. Advanced nanotechnology is used to create new electrode architectures for low Pt loading, such as the 3 M nanostructured thin-film (NSTF) electrode.[2–4] While the mass activity of this novel electrode can be 10 times that of the commercial dispersed Pt/carbon (Pt/C) electrodes,[2] complicated and expensive manufacturing process as well as the water flooding issue at low temperatures may limit its commercialization potential as compared to dispersed Pt/C electrodes.[4]

Further decrease of Pt loading in PEM fuel cells requires a deep understanding of the transport processes of reactants, water, electrons and ions in the catalyst layer (CL), where electrochemical reactions occur, especially at low Pt loadings. Many studies found that the transport resistance increases significantly in electrodes of low Pt loading. Due to the complex structure and small scale of the electrode, direct measurement of the transport resistances has remained an impossible task until now. The indirect method based on the limiting current density has been widely used in recent years to separate the transport resistance in the individual components of the cell.[5–8] For example, by varying the oxygen partial pressure, the total oxygen transport resistance can be divided into a pressure-dependent part and a pressure-independent part, and the latter includes Knudsen diffusion resistance and micro-scale electrode transport resistance near the Pt surface. It was found that the electrode transport resistance increases with the reduction of Pt loading. In measurements of Greszler et al.,[8] the electrode transport resistance is about 0.05 s/cm at 0.4 mg/cm^2 Pt loading but about 0.2 s/cm at 0.1 mg/cm^2 Pt loading. This increase could be due to the decrease of the electrochemically active surface area and subsequent higher fluxes of oxygen through the ionomer film to the catalyst sites.[9] Modeling studies were performed by using the measured local resistance as an input parameter to fit the experimental polarization curves. Ono et al.[10] and Fukuyama et al.[11] concluded that the predicted I-V curves overestimated the experimental results without considering the local resistance, especially at lower Pt loading, indicating that the oxygen transport loss caused by local resistance is marked at low Pt loading. Generally, modeling has been an effective tool to understand transport phenomena in the very thin catalyst layer that are difficult to probe through experimental methods.

The agglomerate model has been commonly used to study the Pt loading effect in the PEM fuel cell electrode. By modeling the agglomerate particles consisting of a mixture of ionomer, carbon particles and carbon-supported platinum particles, the oxygen transport resistance at the micro-scale was introduced in the agglomerates. Such a model introduces additional parameters relating to the electrode structure, such as the agglomerate size and the ionomer film thickness surrounding an agglomerate. The oxygen transport resistance in the agglomerate is a function of these parameters.[12] However, a wide range of agglomerate sizes from 100 nm to 2000 nm, and ionomer thicknesses from 10 nm to 100 nm, had to be assumed in the literature[13–20] as fitting parameters in order to match their experimental data. Such large and random agglomerate size and thick ionomer film were not supported by microscopy observations.[21,22] For a Pt/C electrode, Suzuki et al. found interconnecting particles with diameters from 10 to 50 nm,[21] which is nearly the same as the size of Pt/C particles. Even if regarding the loosely-packed rod-like region as the agglomerate, its diameter is still smaller than 300 nm. Similar electrode morphology was also observed in Greszler's work.[8] Therefore, the agglomerates probably do not exist in reality. Even if non-uniform agglomerates may exist with a size distribution as discussed by Epting and Lister,[23] the diameter of the largest agglomerates may not exceed 300 nm, and these agglomerates occupy only a small percentage of the total catalyst particles.

The thick ionomer film assumed in agglomerate models may not be physical either. Assuming the ionomer is uniformly distributed on the Pt/C particles or surface of small agglomerates, this ionomer film thickness only allows several nanometers given an actual electrode's ionomer to carbon ratio (I/C).[8,21] It is questionable that thick ionomer film (tens to one hundred nanometers) is required to capture the measured local transport resistance. Some research argued a much smaller oxygen diffusivity in the thin ionomer film than that in the bulk membrane in order to obtain a relatively reasonable ionomer thickness.[8,24] Indeed, oxygen diffusivity has not been measured in-situ in very thin film in the catalyst layer. Although a decreased ion conductivity in thin ionomer film was suggested in some studies,[25–27] probably due to the decrease of water uptake with decreasing film thickness, extending this conclusion to oxygen diffusivity remains an open question. Other works, however, showed ion conductivity in the catalyst layer similar to that in the bulk membrane.[28,29] In ex-situ measurements,

*Electrochemical Society Active Member.
zE-mail: cxw31@psu.edu

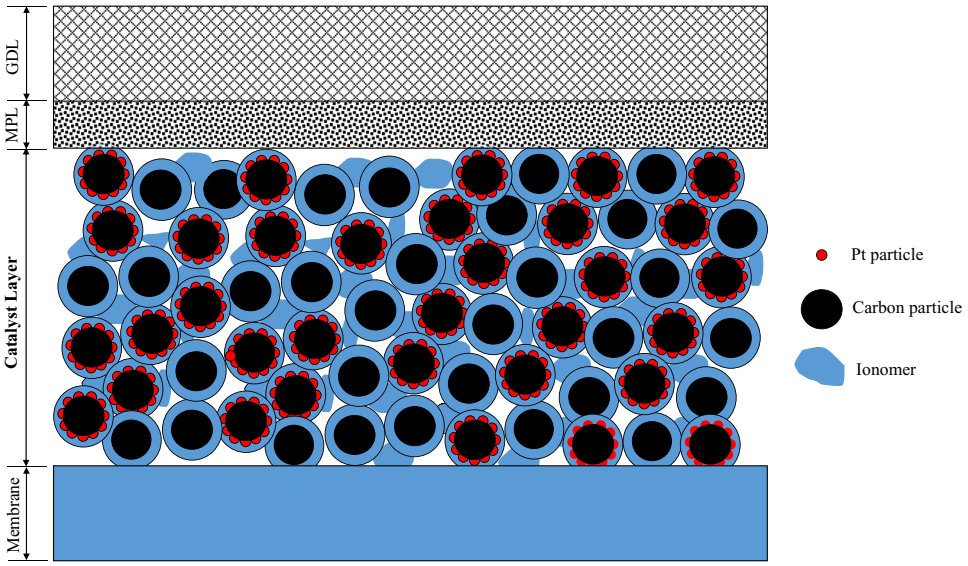

Figure 1. Illustration of the catalyst layer structure.

Kudo et al.[30,31] measured the oxygen dissolution and transport resistance through ionomer films on a Pt substrate. The results showed that the oxygen transport resistance does not deviate from the linear relationship from film thickness of 800 nm to 25 nm, indicating a similar oxygen diffusivity in this large thickness range. They introduced an interfacial resistance at the ionomer surface by assuming an oxygen dissolution resistance there and fitted a reasonable, small agglomerate size for their model. The most recent study,[32] however, demonstrated that the dissolution resistance has little impact on the cell performance, using Kudo et al.'s experimental data.[30,31] Much controversy remains as to exact physical origins of the local micro-scale oxygen transport resistance at low Pt loading.

The local transport resistance in the catalyst layer depends not only on the Pt loading but also on the electrode composition. Owejan et al.[33] recently reported several sets of experiments by diluting various wt% Pt catalyst material with bare carbon support, while keeping constant Pt loading with same electrode thickness. The measured data showed that performance loss increases with increased carbon dilution fraction at a given Pt loading, especially at Pt loading lower than 0.1 mg/cm^2. This work stresses that the electrode structure is more complicated than only considering the Pt loading effect. The distribution of the catalyst particles, i.e. Pt particles, may have significant impact on fuel cell performance as well. However, both the experimental and modeling studies on this issue are still limited.

In this work, a comprehensive electrode model is proposed taking both the Pt loading and electrode composition into consideration, and coupled into a macro-scale PEM fuel cell model. The effect of Pt loading and electrode compositions with and without carbon dilution on PEM fuel cell performance is examined and validated with extensive experimental data under different operating conditions from Owejan et al.[33] The present electrode model does not consider the agglomerates for the reasons discussed earlier; however, in the final part of this work, this assumption is examined by further extending the present model into an agglomerate model to study the agglomerate size effect.

Electrode Model

The catalyst layer is composed of gas pores, carbon particles, Pt catalyst particles and the ionomer network. We further assume solid carbon particles as validation shall be performed against the experiments of Owejan et al.[33] that used Vulcan carbon support. Fig. 1 schematically illustrates the catalyst layer structure including both the activated Pt/C particles and the bare carbon particles as the diluent. Pt particles disperse on the carbon particle surface. The ionomer in the catalyst layer forms a film covering the Pt/C or bare carbon particles and connects them together to form an ionic network. The catalyst layer possibly has a few small agglomerates or none. For the latter case, we develop a homogeneous porous electrode model, and for the former case we shall justify the assumption of neglecting agglomerates in a later section.

Transport resistance near Pt/C particles.— As shown in Fig. 1, the catalyst layer is assumed to consist of independent particles covered by an ionomer film with the thickness δ_e. For a single Pt/C particle, we depict the oxygen concentration profile in Fig. 2. Reactant oxygen in the gas phase will first dissolve into the ionomer. According to Henry's law, the equilibrium concentration of oxygen $C^1_{o_2}$ in the ionomer is,

$$C^1_{o_2} = \frac{RT}{H_{o_2,\mathrm{e}}} C^g_{o_2} \qquad [1]$$

where $H_{o_2,e}$ is the Henry constant of oxygen at the ionomer surface. Because the oxygen dissolution rate in ionomer is not unlimited, a dissolution resistance at the interface exists.[30,31] The oxygen flux N_{o_2}

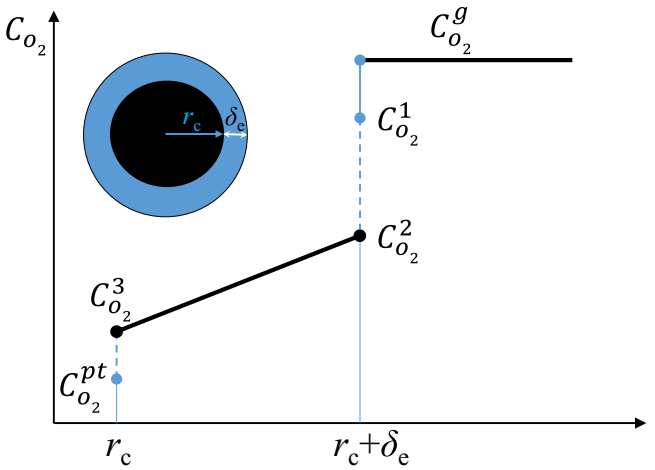

Figure 2. Schematic of the oxygen concentration profile near a catalyst particle.

across the ionomer surface is given by,

$$N_{o_2} = \frac{1}{R_{\text{e,dissol}}}\left(C^1_{o_2} - C^2_{o_2}\right) \quad [2]$$

where $R_{\text{e,dissol}}$ is the non-equilibrium dissolution resistance and depends on the dissolution rate for oxygen in the ionomer.

Through the thin ionomer film, the oxygen flux is described by one dimensional Fick's equation (this is a reasonable approximation for an ionomer film of several nanometers thick as compared to ~25 nm of carbon particle radius),

$$N_{o_2} = \frac{D_{o_2,\text{ion}}}{\delta_e}\left(C^2_{o_2} - C^3_{o_2}\right) \quad [3]$$

where $D_{o_2,\text{ion}}$ is the oxygen diffusivity in the ionomer film and $C^3_{o_2}$ is the oxygen concentration near the carbon particle surface.

In addition, an interfacial resistance may also exist at the Pt surface due to the modification of the Pt atoms and ionomer structure at Pt/ionomer interface by sulfonate ion absorption, which leads to the decrease of the effective Pt surface area and decease of the oxygen permeability.[34] It follows that the oxygen flux near the Pt surface can be written as

$$N_{o_2} = \frac{1}{R_{\text{pt,int}}}\left(C^3_{o_2} - C^{pt}_{o_2}\right) \quad [4]$$

where $C^{pt}_{o_2}$ is the oxygen concentration at the Pt surface and $R_{\text{pt,int}}$ is the interfacial transport resistance near the Pt surface.

The above expressions of the transport resistances near the Pt/C particle assume a perfect and uniform coverage of the ionomer. However, actual ionomer distribution appears to be heterogeneous, from relatively thick coverage to non-coverage.[22] It is more convenient to combine Equation 1 and 2 into a single interfacial resistance if assuming a uniform ionomer coverage, which is,

$$N_{o_2} = \frac{1}{R_{\text{e,int}}}\left(C^g_{o_2} - C^2_{o_2}\right) \quad [5]$$

where $R_{\text{e,int}}$ is the integrated interfacial transport resistance at the pore/ionomer interface.

From Equation 3 through Equation 5, we get the relationship between the oxygen concentration in gas phase and on the Pt surface,

$$\left(R_{e,\text{int}} + \frac{\delta_e}{D_{o_2,ion}} + R_{pt,\text{int}}\right) N_{o2} = C^g_{o_2} - C^{pt}_{o_2} \quad [6]$$

It should be noted that Equation 6 reflects the ionomer film effect on oxygen transport resistance. On the other hand, if liquid water exists in the catalyst layer, the liquid water would prefer to cover the ionomer surface because of its hydrophilic characteristic.[22] A similar equation can be written to describe the oxygen transport resistance through a water film, as was done for that in ionomer film, and the total transport equation through both water and ionomer films is,

$$\left(R_{w,\text{int}} + \frac{\delta_w}{D_{o_2,w}} + R_{e,\text{int}} + \frac{\delta_e}{D_{o_2,ion}} + R_{pt,\text{int}}\right) N_{o_2} = C^g_{o_2} - C^{pt}_{o_2} \quad [7]$$

where $R_{w,\text{int}}$ is the transport resistance at the water film surface, δ_w is the water film thickness and $D_{o_2,w}$ is the oxygen diffusivity in water film.

The oxygen flux across the water and ionomer films is related to the local reaction rate. Based on Subramanian et al.'s work,[35] the Pt-oxide-coverage-dependent kinetics equation for oxygen reduction reaction (ORR) is given by,

$$j_c = -i_{0,c} a_{\text{pt}}(1-\theta_{\text{PtO}})\left(\frac{C^{pt}_{O2}}{C_{O_2,ref}}\right)^{\gamma} \exp\left(-\frac{\alpha_c}{RT}F\eta_c - \frac{\omega\theta_{\text{PtO}}}{RT}\right) \quad [8]$$

$$i_{0,c} = i^{ref}_{0,c} \exp\left(-\frac{E_c}{R}\left(\frac{1}{T} - \frac{1}{353.15}\right)\right) \quad [9]$$

where ω is the energy parameter for the Temkin isotherm, γ is the reaction order in ORR, a_{pt} is the active volumetric surface area of Pt which is related to the Pt loading L_{pt} and electrochemical specific area (ECSA) of Pt particles a_{ECSA}, by,

$$a_{\text{pt}} = \frac{a_{\text{ECSA}} L_{\text{pt}}}{\delta_{\text{CL}}} \quad [10]$$

Here δ_{CL} is the thickness of the catalyst layer.

The Pt-oxide coverage θ_{PtO} is fitted from the experimental data in Ref. 35 and can be expressed by,

$$\theta_{\text{PtO}} = 1/\left(1 + e^{22.4(0.818-E)}\right) \quad [11]$$

where E is the cathode potential vs. RHE.

As mentioned before, the catalyst layer may have both Pt/C catalyst particles and bare carbon particles, as shown in Fig. 1. The bare carbon is inactive for ORR, so the effective specific surface area of the ionomer on Pt/C particles is given by,

$$a^{eff}_c = a_c x = n_c A_c x \quad [12]$$

where $a_c = n_c * A_c$ is the volumetric surface area of ionomer, n_c is the total number of the Pt/C particles and bare carbon particles per volume, A_c is the ionomer surface area for one particle and x is the number fraction of the Pt/C particles. Equation 12 assumes that the Pt/C particle and the bare carbon particle have the same size because the much smaller Pt particles dispersed on carbon support almost do not change the carbon size. If further assuming spherical shape of these particles, we have,

$$n_c = \frac{\varepsilon_c}{\frac{4}{3}\pi {r_c}^3} \quad [13]$$

$$A_c = 4\pi(r_c + \delta_e)^2 \quad [14]$$

$$a_c = \frac{3\varepsilon_c}{{r_c}^3}(r_c + \delta_e)^2 \quad [15]$$

where ε_c is the volume fraction of the carbon particle in the catalyst layer and r_c is the carbon particle radius.

For a Pt/C catalyst particle, the oxygen flux around it is given by,

$$N_{o2} = -\frac{i_{c,\text{Pt/C}}}{4F} = -\frac{j_c}{4F a_c x} \quad [16]$$

Substitute the oxygen flux Equation 16 into Equation 7, we have,

$$-\left(R_{w,\text{int}} + \frac{\delta_w}{D_{o_2,w}} + R_{e,\text{int}} + \frac{\delta_e}{D_{o_2,ion}} + R_{pt,\text{int}}\right)\frac{j_c}{4F a_c x} = C^g_{o_2} - C^{pt}_{o_2} \quad [17]$$

If we define the following parameters,

$$A = R_{w,\text{int}} + \frac{\delta_w}{D_{o_2,w}} + R_{e,\text{int}} + \frac{\delta_e}{D_{o_2,ion}} + R_{pt,\text{int}}$$

$$D = i_{0,c} a_{pt}(1-\theta_{\text{PtO}})\left(\frac{1}{C_{O_2,ref}}\right)^{\gamma} \exp\left(-\frac{a_c}{RT}F\eta_c - \frac{\omega\theta_{\text{PtO}}}{RT}\right)$$

Then Equation 17 can be rewritten by,

$$D\left(C^{pt}_{o_2}\right)^{\gamma} + \frac{4F}{A/(a_c x)}C^{pt}_{o_2} - \frac{4F}{A/(a_c x)}C^g_{o_2} = 0 \quad [18]$$

For the first order reaction, where $\gamma = 1$, Equation 18 can be solved analytically. However, a numerical method is needed for Equation 18 if the reaction order γ is smaller than 1.

The above model assumes that the Pt particles completely cover the carbon particle surface, as used in prior homogeneous and agglomerate models in literature. This should be valid for high wt% Pt catalyst materials. However, for the low wt% Pt catalyst material, the Pt particles are distributed in a more dispersed manner on the carbon particle, resulting in a longer oxygen diffusion path than the ionomer film thickness. As indicated in a 2D simplified particle model conducted by Yoon and Weber,[12] the oxygen diffusion path increases as the number of active sites or Pt particles on carbon support decreases.

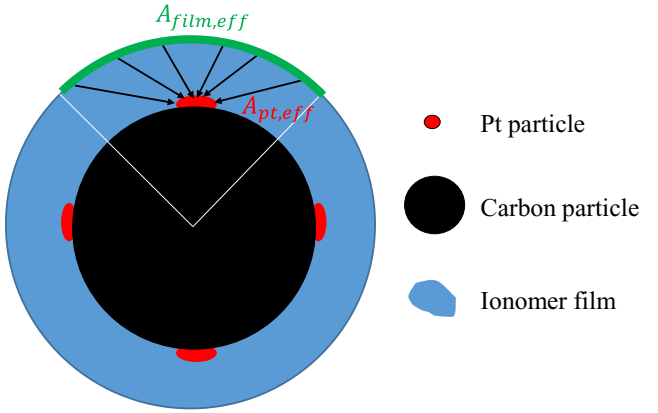

Figure 3. Schematic of the oxygen diffusion path through the ionomer film on a Pt/C particle.

Assuming Pt particles having the spherical shape with the same size, the Pt particle number on a Pt/C carbon particle can be estimated by,

$$n_{pt} = \frac{\rho_c}{\rho_{pt}} \left(\frac{r_c}{r_{pt}}\right)^3 \left(\frac{wt\%}{1 - wt\%}\right) \quad [19]$$

where $wt\%$ is the Pt weight percentage of the Pt/C catalyst material (not the overall weight percentage of the catalyst layer). ρ_c and ρ_{pt} are carbon and Pt densities, respectively. The Pt particle radius r_{pt} can be expressed by,[33]

$$r_{pt} = \frac{3}{\rho_{pt} \cdot a_{ECSA}} \quad [20]$$

If the Pt particles are uniformly distributed on the carbon particle surface, as shown in Fig. 3, the effective surface area of a Pt particle $A_{pt,eff}$ and the effective ionomer surface area available for one Pt particle $A_{film,eff}$ are calculated by,

$$A_{pt.eff} = 4\pi r_{pt}^2 (1 - \theta_{PtO}) \quad [21]$$

$$A_{film.eff} = \frac{4\pi (r_c + \delta_e)^2}{n_{pt}} \quad [22]$$

Obviously, the effective diffusion length of oxygen from the ionomer surface to the Pt particle is longer than the ionomer film thickness when $A_{film,eff}$ is larger than $A_{pt,eff}$ for a sparse Pt particle distribution. In Equation 21, the Pt-oxide coverage is excluded because of no activation there.

If we consider that the oxygen flux in Equation 3–5 is based on the flux scaling to the ionomer surface, the effective diffusion length can be approximately obtained by,

$$\delta_{eff} = \frac{A_{film,eff}}{A_{pt,eff}} \delta_e = \frac{(r_c + \delta_e)^2 / n_{pt}}{r_{pt}^2 (1 - \theta_{PtO})} \delta_e \quad [23]$$

In addition, the interfacial transport resistance near the Pt surface $R_{pt,int}$ should also be revised when scaling the flux to the ionomer surface, which is,

$$R_{pt,int,\text{eff}} = \frac{A_{film,eff}}{A_{pt,eff}} R_{pt,int} = \frac{(r_c + \delta_e)^2 / n_{pt}}{r_{pt}^2 (1 - \theta_{PtO})} R_{pt,int} \quad [24]$$

Substitute Equation 19 into 23 and 24, we have,

$$\delta_{eff} = \frac{(r_c + \delta_e)^2}{r_{pt}^2 (1 - \theta_{PtO})} \frac{\rho_{pt}}{\rho_c} \left(\frac{r_{pt}}{r_c}\right)^3 \left(\frac{1 - wt\%}{wt\%}\right) \delta_e \quad [25]$$

$$R_{pt,int,\text{eff}} = \frac{(r_c + \delta_e)^2}{r_{pt}^2 (1 - \theta_{PtO})} \frac{\rho_{pt}}{\rho_c} \left(\frac{r_{pt}}{r_c}\right)^3 \left(\frac{1 - wt\%}{wt\%}\right) R_{pt,int} \quad [26]$$

Notice that Equation 26 applies only to a Pt/C catalyst particle. In this case, a lower wt% means less Pt loading, and thus a higher interfacial transport resistance.

Using the effective diffusion length δ_{eff} and the scaled interfacial transport resistance $R_{pt,int,eff}$ instead of δ_e and $R_{pt,int}$ in Equation 17, the Pt weight percentage effect of the Pt/C material on oxygen transport resistance is taken into account. Finally, the oxygen concentration difference between $C_{o_2}^g$ and $C_{o_2}^{pt}$ is obtained as,

$$C_{o_2}^g - C_{o_2}^{pt} = -\left[R_{w,\text{int}} + \frac{\delta_w}{D_{o_2,w}} + R_{e,\text{int}} + \frac{(r_c + \delta_e)^2}{r_{pt}^2 (1 - \theta_{PtO})} \frac{\rho_{pt}}{\rho_c} \left(\frac{r_{pt}}{r_c}\right)^3 \times \left(\frac{1 - wt\%}{wt\%}\right) \left(R_{pt,\text{int}} + \frac{\delta_e}{D_{o_2,ion}}\right)\right] \frac{j_c}{4F a_c x} \quad [27]$$

The three interfacial resistances in the above equation are unknown. If we estimate them by the following simple formulas,

$$R_{e,\text{int}} = k_1 \frac{\delta_e}{D_{o_2,ion}}; \quad R_{pt,\text{int}} = k_2 \frac{\delta_e}{D_{o_2,ion}}; \quad R_{w,\text{int}} = k_3 \frac{\delta_w}{D_{o_2,w}} \quad [28]$$

then, Equation 27 becomes,

$$C_{o_2}^g - C_{o_2}^{pt} = -\left[(k_3 + 1) \frac{\delta_w}{D_{o_2,w}} + \left(k_1 + \frac{(r_c + \delta_e)^2}{r_{pt}^2 (1 - \theta_{PtO})} \frac{\rho_{pt}}{\rho_c} \left(\frac{r_{pt}}{r_c}\right)^3 \times \left(\frac{1 - wt\%}{wt\%}\right) (k_2 + 1)\right) \frac{\delta_e}{D_{o_2,ion}}\right] \frac{j_c}{4F a_c x} \quad [29]$$

Substituting Equation 15 and 20 into Equation 29, we get the total transport resistance near a Pt/C particle,

$$R_T = -\frac{4F\left(C_{o_2}^g - C_{o_2}^{pt}\right)}{j_c \cdot \delta_{CL}} = \left[(k_3 + 1) \frac{\delta_w}{D_{o_2,w}} \frac{a_{ECSA}}{a_c f_t} + \left(k_1 \frac{a_{ECSA}}{a_c f_t} + \frac{k_2 + 1}{1 - \theta_{PtO}} \left(\frac{1 - wt\%}{wt\%}\right)\right) \frac{\delta_e}{D_{o_2,ion}}\right] \frac{f_t}{a_{ECSA} \delta_{CL}} \frac{1}{x} \quad [30]$$

Here, $f_t = 1/(\varepsilon_c\, \rho_c)$ is the factor of catalyst layer thickness from carbon loading and this value is about 28 μm/(mg$_c$/cm^2) for the electrode with ionomer/carbon (I/C) weight ratios smaller than 3.[36]

In addition, the Pt loading can be calculated by,

$$L_{pt} = x \cdot n_c \cdot \delta_{CL} \cdot n_{pt} \cdot \frac{4}{3} \pi r_{pt}^3 \cdot \rho_{pt} = x \frac{\delta_{CL}}{f_t} \frac{wt\%}{1 - wt\%} \quad [31]$$

Combing Equation 30 and 31, we have,

$$R_T = (k_2 + 1) \frac{\delta_e}{D_{o_2,ion}} \frac{1}{(1 - \theta_{PtO}) a_{ECSA} L_{pt}} + \left[k_1 \frac{\delta_e}{D_{o_2,ion}} + (k_3 + 1) \frac{\delta_w}{D_{o_2,w}}\right] \frac{1}{\delta_{CL} a_c x} \quad [32]$$

Note that Equation 32 takes into account the Pt loading effect and catalyst particles fraction effect, respectively, and that the transport resistance R_T increases with the decrease of Pt loading L_{pt} and Pt/C catalysts fraction x in the electrode. Therefore, this new catalyst layer model captures the role of the catalyst composition on oxygen transport resistance in addition to the Pt loading.

In the above analysis, a single catalyst material with uniform Pt weight percentage is assumed. However, blended Pt/C materials with differing wt% may be used in actual catalyst layer fabrication. For such a blended catalyst layer, Equation 32 is also valid (see detail in Appendix A) with x being the total catalyst particle number fraction,

which can be expressed by,

$$x = \frac{(1 - wt_{\text{avg}}\%)(1 - y_{\text{bare}})}{1 - wt_{\text{avg}}\%(1 - y_{\text{bare}})} \quad [33]$$

where $wt_{\text{avg}}\%$ is the average Pt weight percentage of the Pt/C catalyst and is given by,

$$wt_{\text{avg}}\% = \frac{\sum_N y_i wt_i\%}{\sum_N y_i} \quad [34]$$

In Equation 33 and 34, y_{i} and y_{bare} are the weight fraction of the catalyst type i and bare carbon, respectively, and N is the number of the catalyst types.

Structural parameters of catalyst layer.— Structural parameters of the catalyst layer, such as carbon particle fraction, ionomer film thickness, carbon particle size, and ionomer volumetric surface area are incorporated as inputs in the above transport resistance analysis. Moreover, other parameters, such as porosity, pore size and ionomer fraction, are needed to evaluate the effective transport properties in the porous electrode. These parameters should not be arbitrarily specified but dependent upon the catalyst layer design and fabrication.

The size of the commonly used Vulcan XC-72 carbon support is ~25 nm. Given the carbon loading L_{c}, the volume fraction of carbon particles can be estimated by,

$$\varepsilon_c = \frac{1}{\rho_c}\frac{L_c}{\delta_{CL}} \quad [35]$$

As mentioned above, the effective electrode thickness $\delta_{\text{CL}}/L_{\text{c}}$ is about 28 μm/(mg$_{\text{c}}$/cm^2) for I/C ratios smaller than 3.[36] From this value, the thickness of a catalyst layer with Pt loading of 0.4 mg/cm^2 is about 11.2 μm when using pure 50% wt Pt/Vulcan catalyst.

Using Equation 35, the volume fraction of ionomer in the catalyst layer is,

$$\varepsilon_e = (I/C)\,\varepsilon_c \frac{\rho_c}{\rho_e} \quad [36]$$

where ρ_{e} is the density of ionomer. The volume of ionomer expands with water uptake, so the above equation should be revised by an expansion factor in wet conditions,[36] which is,

$$\varepsilon_e = (I/C)\,\varepsilon_c \frac{\rho_c}{\rho_e}\left(1 + \frac{M_w \rho_e}{\rho_w EW}\lambda\right) \quad [37]$$

where ρ_{w} is the water density, EW is the ionomer equivalent weight and λ is the water content in ionomer.

The porosity of the catalyst layer is,

$$\varepsilon_{CL} = 1 - \varepsilon_c - \varepsilon_e \quad [38]$$

From geometry analysis, the ionomer volume fraction can also be expressed by,

$$\varepsilon_e = \frac{4}{3}\pi\left[(r_c + \delta_e)^3 - r_c^3\right] n_c \quad [39]$$

Substitute Equation 13 of n_{c} into Equation 39, the ionomer thickness surrounding the carbon particles is estimated by,

$$\delta_e = \left(\left(\frac{\varepsilon_e}{\varepsilon_c} + 1\right)^{1/3} - 1\right) r_c \quad [40]$$

The pore size in catalyst layer r_{p} can be estimated according to the same specific surface area of ionomer from the particle side and pore side, which is,

$$a_c = \frac{3(1 - \varepsilon_{\text{CL}})}{r_c + \delta_e} = \frac{3\varepsilon_{\text{CL}}}{r_p} \quad [41]$$

From Equation 41, we have,

$$r_p = \frac{\varepsilon_{\text{CL}}}{1 - \varepsilon_{\text{CL}}}(r_c + \delta_e) \quad [42]$$

Table I. Input parameters for catalyst layer structure parameters estimation.

Parameters	Value	Unit
ρ_{c}	1.95	g/cm^3
ρ_{Pt}	21.45	g/cm^3
ρ_{w}	1.0	g/cm^3
ρ_{e}	1.9	g/cm^3
M_{w}	18.0	g/mol
EW	950.0	g/mol
a_{ECSA}	70	m^2$_{\text{-pt}}$/g$_{\text{pt}}$
r_c	25	nm
I/C	0.6 (anode) / 0.95 (cathode)	-

Therefore, the estimated pore radius in the catalyst layer has the same order as the carbon particle.

The inputs for catalyst layer structural parameters estimated from the above equations are listed in Table I.

PEM Fuel Cell Model

The present electrode model described above is integrated into a full-cell PEM fuel cell model, i.e. M2 model.[37] This model simulates mass, momentum, energy, species and charge transport processes, under either single- or two-phase conditions, throughout a PEM fuel cell. The governing equations can be summarized as follows:

$$\text{Continuity equation} \quad \nabla \cdot (\rho\vec{u}) = 0 \quad [43]$$

$$\text{Momentum conservation} \quad \nabla \cdot \left(\frac{\rho\vec{u}\vec{u}}{\varepsilon^2}\right) = -\nabla P + \nabla \cdot (\mu\nabla\vec{u}) + S_u \quad [44]$$

$$\text{Energy conservation} \quad \nabla \cdot (\gamma_T \rho c_p \vec{u} T) = \nabla \cdot (k^{eff}\nabla T) + S_T \quad [45]$$

Species conservation

$$\nabla \cdot \left(\gamma_C \vec{u} C^i\right) = \nabla \cdot \left(D_g^{i,eff}\nabla C_g^i\right) - \nabla \cdot \left[\left(\frac{m f_l^i}{M^i} - \frac{C_g^i}{\rho_g}\right)\vec{j}_l\right] + S_C^i \quad [46]$$

$$\text{Electron conservation} \quad 0 = \nabla \cdot \left(\sigma_s^{eff}\nabla\Phi_s\right) - j \quad [47]$$

$$\text{Proton conservation} \quad 0 = \nabla \cdot \left(\kappa_e^{eff}\nabla\Phi_e\right) + j \quad [48]$$

where, ρ, $\vec{u}$, P, T, C^i, Φ_{s} and Φ_{e} are the density, superficial fluid velocity vector, pressure, temperature, molar concentration of species i, electronic phase potential, and electrolyte phase potential, respectively. For more detail about this model, refer to reference 37. j in Equation 47 and 48 is the reaction current. The oxygen reduction reaction current in the cathode catalyst layer is given by Equation 8 and 9, and the hydrogen oxidation reaction current in anode side is,

$$j_a = a_{\text{pt}} i_{0,\text{a}}^{ref} \exp\left(-\frac{E_a}{R}\left(\frac{1}{T} - \frac{1}{353.15}\right)\right)\left(\frac{C_{H_2}^{pt}}{C_{H_2,ref}}\right)^{\gamma}\frac{\alpha_a}{RT}F\eta \quad [49]$$

The parameters for electrode kinetics are listed in Table II.

Transport parameters.— The effective transport coefficients in various porous components of a PEM fuel cell are functions of their structural parameters. In GDL, the effective diffusivities of the species are assumed following the Bruggeman approximation, which are,

$$D_g^{i,eff} = \frac{\varepsilon_k}{\tau_k} D_g^i \quad [50]$$

where ε_{k} and τ_{k} are the porosity and tortuosity of the porous material, D_g^i is the molecular diffusion coefficient of the species i.

Table II. Parameters for electrochemical kinetics.[35,38]

Parameters	Value	Unit
Anode side		
$i_{0,a}^{ref}$	0.3	A/cm^2-Pt
E_a	10.0	kJ/mol
$C_{H2,ref}$	4.0e-5	mol/cm^3
γ	0.5	-
α_a	2.0	-
Cathode side		
$i_{0,c}^{ref}$	3.0e-5	A/cm^2-Pt
E_c	67.0	kJ/mol
$C_{O2,ref}$	4.0e-5	mol/cm^3
γ	0.7	-
α_c	0.5	-
ω	3.0	kJ/mol

In the catalyst layer, where the pore size is smaller than 100 nm, the Knudsen diffusion is important and the species diffusivity can be calculated by the following equation,

$$D^i = (1/D_g^i + 1/D_{Knud}^i)^{-1} \quad [51]$$

with the Knudsen diffusion coefficient evaluated as,

$$D_{Knud}^i = \frac{2r_p}{3}\left(\frac{8RT}{\pi M_i}\right)^{1/2} \quad [52]$$

Here, r_p is the radius of the pore size and M_i is the molar mass of the species i.

The proton conductivity of ionomer in the catalyst layer is fitted from the measured data in Ref. 36 and given by,

$$\kappa = 22.0\exp\left(-\frac{E_\kappa}{R}\left(\frac{1}{T}-\frac{1}{353.15}\right)\right)a^{2.24} \quad [53]$$

where a is the water activity and E_κ is the activation energy with the value of 12 kJ/mol. In addition, the measured tortuosity of the ionomer phase in the catalyst layer in Ref. 36 is given by,

$$\tau_e = \begin{cases} 0.0845(\varepsilon_e - 0.04)^{-1.17} & \varepsilon_e < 0.16 \\ 1.0 & \varepsilon_e \geq 0.16 \end{cases} \quad [54]$$

The water uptake in ionomer is described by Mittlesteadt et al.'s formula:[39]

$$\lambda = \begin{cases} \left[1 + 0.2325a^2\left(\frac{T-303}{30}\right)\right]\left[14.22a^3 - 18.92a^2 + 13.41a\right] & a \leq 1 \\ 8.71\left[1 + 0.2325\left(\frac{T-303}{30}\right)\right](1-s) + (9.22 + 0.181\,(T-273.15))\,s & a > 1 \end{cases} \quad [55]$$

Mittlesteadt et al.[39] also developed a formula of oxygen permeability in ionomer, which accounts for the relative humidity effect. This formula is used in the present work,

$$p_{o_2} = p_{dry}\exp(-E_{dry}/RT) + \upsilon_w p_{wet}\exp(-E_{wet}/RT) \quad [56]$$

where p_{dry} and p_{wet} are the permeability for dry and wet phases, E_{dry} and E_{wet} are the activation energy for oxygen transport in wet and dry phases, and υ_w is the volume fraction of water in ionomer. The values and expression of these parameters are: $p_{dry} = 0.674 \times 10^{-11}$ mol/(m Pa s), $p_{wet} = 5.05 \times 10^{-11}$ mol/(m Pa s), $E_{dry} = 21.28$ kJ/mol, $E_{wet} = 20.47$ kJ/mol, and $\upsilon_w = 18\lambda/(18\lambda + EW/\rho_e)$.

The water permeability in membrane is given by,[40]

$$p_w = 3.2 \times 10^{-11}\exp\left[\frac{E_w}{R}\left(\frac{1}{T}-\frac{1}{363}\right)\right]\exp(3.4a) \quad [57]$$

where the activation energy $E_w = 22$kJ/mol.

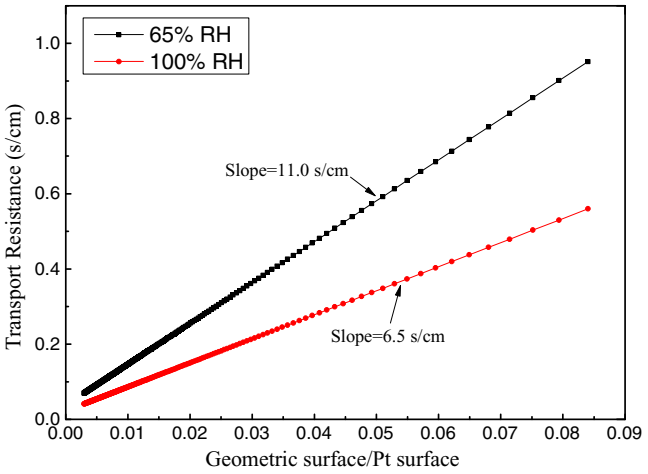

Figure 4. Predicted electrode transport resistance with geometric surface/Pt surface ratio ($1/(a_{ECSA} * L_{pt})$) by equation 32 with $\delta_w = 0$, $x = 1$, $k_1 = 8.5$ and $k_2 = 5.4$.

Numerical Procedures

Most of the prior works to study Pt loading effect on PEM fuel cell performance only focused on the catalyst layer using a one-dimensional model. In the present work, we perform a full-cell 3D simulation by solving the governing equations 43–48, meanwhile, coupling the catalyst layer sub-model in every node of the cathode catalyst layer. Hence, the present model can handle a 3D automotive fuel cell with the low-Pt loading catalyst layer.

Results and Discussion

According to the analysis of Greszler et al.,[8] the electrode transport resistance excluding the diffusion resistance in macro-pores can be scaled inversely with the roughness factor (defined as the Pt surface area per electrode geometrical area). It is noted from our present electrode model, i.e. Equation 32, that the electrode transport resistance as a function of the ratio of geometric surface/Pt surface, which is $1/(a_{ECSA}L_{pt})$, shows an obvious linear relationship in Fig. 4 for constant catalyst material fraction x. Two different relative humidity (RH) conditions, i.e. 65% and 100%, are plotted, where the oxygen diffusivity is calculated by Equation 56. The slope of the line is the scaled local transport resistance, which is defined as electrode transport resistance multiplying roughness factor. We assume the two interfacial resistance coefficients k_1 and k_2 to be 8.5 and 5.4, respectively. $k_1 = 8.5$ falls into the range of ionomer interfacial resistance to ionomer diffusion resistance measured by Kudo et al.[30,31] and is close to their average value. The interfacial resistance near the Pt surface has no measured data in the literature. We set its value at 5.4, which results in the local transport resistance of 11.0 s/cm and 6.5 s/cm for 65% RH and 100% RH, respectively. It should be noted that 11.0 s/cm falls into the in-situ measured range in Greszler et al.'s[8] limiting current experiments under a similar RH of 62%. Therefore, it is expected that the present electrode transport model predicts the local transport resistance in good agreement with the experimental data in the literature.

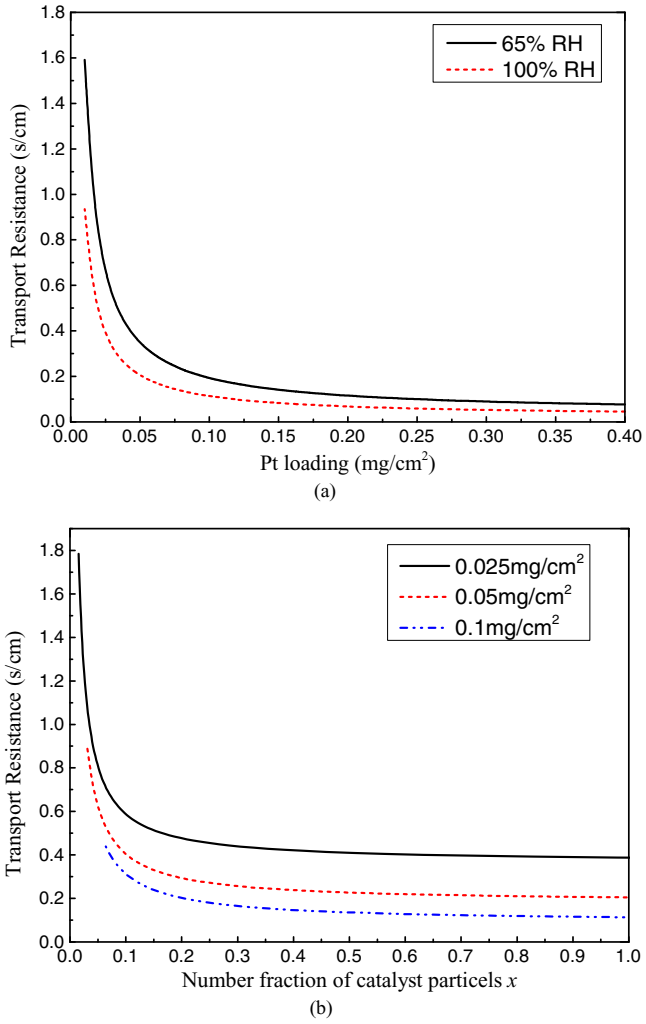

Figure 5. (a) Electrode transport resistance with Pt loading for non-diluted catalyst material ($x = 1$) under RH = 65% and RH = 100%, and (b) electrode transport resistance with catalyst particle number fraction for Pt loading of 0.025 mg/cm^2, 0.5 mg/cm^2 and 0.1 mg/cm^2 under RH = 100%.

In this work, $k_1 = 8.5$ and $k_2 = 5.4$ are used in all of the following simulations. Using Equation 32, the electrode transport resistance with Pt loading and catalyst particle number fraction are plotted in Fig. 5a and 5b, respectively. As reported in some experimental works, Fig. 5a shows that the electrode transport resistance increases significantly with Pt loading lower than 0.1 mg/cm^2. Moreover, higher transport resistance is also observed for higher carbon dilution at a given Pt loading, as shown in Fig. 5b. These figures quantify the effects of not only the Pt loading but also electrode compositions.

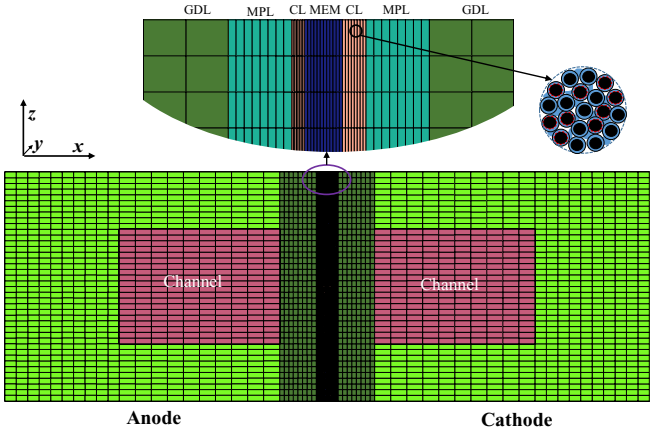

Figure 6. Geometry and computational mesh.

Table IV. Geometry parameters of the differential cell.[33]

Parameters	Value	Unit
Membrane thickness	18	μm
CCL thickness	11	μm
ACL thickness	6	μm
MPL thickness	30	μm
GDL thickness	160	μm
Channel width	0.5	mm
Channel height	0.7	mm
Land width	0.5	mm

A series of simulation studies are subsequently conducted to compare the predicted and measured polarization curves for a wide range of Pt loadings and electrode compositions. In the experiments of Owejan et al.,[33] two electrode compositions were used for the cathode catalyst layers: (1) without bare carbon dilution; (2) with bare carbon dilution. All these catalyst layers were designed to have the same thickness, i.e. ~11 μm, by controlling the fraction of the electrode components. In addition, all samples used Pt/Vulcan catalyst and Vulcan XC-72 carbon as the diluent. The anode catalyst layer has the same Pt loading of 0.05 mg/cm^2 and the I/C ratio was maintained to be 0.6 and 0.95 in anode and cathode catalyst layer, respectively. Table III lists the Pt loading and the corresponding components of the catalyst layer samples examined in the present work. Owejan et al. used a small MEA of 5 cm^2 in their experiments and used very high stoichiometry of hydrogen and oxygen, so it is appropriate to use a differential cell (i.e. 2D cell with negligible variation along the gas flow direction) to perform the full cell simulations. Fig. 6 shows the geometry and mesh of this differential cell, whose geometrical parameters are given in Table IV. The operating temperature and pressure in all of the following simulations are set at 80 °C and 150 kPa.

No carbon dilution.— Fig. 7 shows the comparison of the predicted and experimental polarization curves for the non-diluted electrodes

Table III. Cathode catalyst layer Pt loading and components.[33]

Case	Pt Loading mg/cm^2	Carbon dilution	Bare carbon mass fraction[a]	Catalyst Type[b]	Catalyst mass fraction	Catalyst particles number fraction
1	0.2	N	-	50%$_{wt}$ /20%$_{wt}$	0.56 /0.44	1.0
2	0.1	N	-	30%$_{wt}$ /15%$_{wt}$	0.29 /0.71	1.0
3	0.05	N	-	10%$_{wt}$	1.0	1.0
4	0.025	N	-	5%$_{wt}$	1.0	1.0
5	0.1	Y	0.58	50%$_{wt}$	0.42	0.265
6	0.05	Y	0.78	50%$_{wt}$	0.22	0.123
7	0.025	Y	0.89	50%$_{wt}$	0.11	0.055

[a]Vulcan XC-72 carbon; [b] Pt/Vulcan (TKK) catalyst.
Anode catalyst layer Pt loading 0.05 mg/cm^2; anode I/C ratio 0.6; cathode I/C ratio 0.95 for all cases.

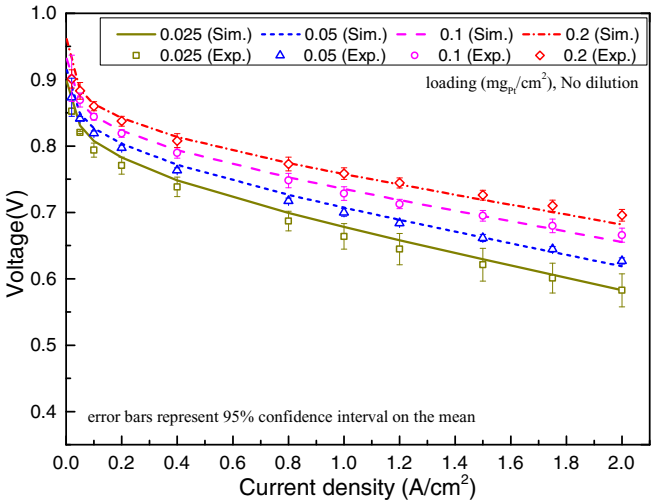

Figure 7. Comparison of polarization curves between experiments and simulations for non-diluted catalyst under pure oxygen, 100% RH, 80 °C and 150 kPa operating condition.

with pure oxygen in the cathode side. There is good agreement from high (0.2 mg/cm^2) to low (0.025 mg/cm^2) Pt loading. Because of the high oxygen concentration with pure oxygen feed, the cells operate in the ohmic region until current density of 2.0 A/cm^2. Lower cell performance with decreasing Pt loading results from the kinetic loss. The distribution of oxygen concentration in catalyst layer pores and on the Pt surface, as well as the distributions of oxygen concentration drop around the Pt particle and oxygen reduction reaction (ORR) current density are plotted in Figs. 8a and 8b for Pt loading of 0.2 mg/cm^2 and 0.025 mg/cm^2, respectively. It should be noted that the catalyst layers have the same thickness of ~11 μm for the two different Pt loadings as mentioned earlier. Evidently, Pt loading has negligible effect on the pore concentration, but has significant influence on the concentration at the Pt surface. However, due to pure oxygen condition, oxygen concentration at the Pt surface is still so high that the mass transfer is not a limitation for ORR.

The predicted polarization curves and HFR for non-diluted electrodes also show good agreement with the experimental data for air feed, as shown in Figs. 9a and 9b. Under the same operating conditions, air feed instead of pure oxygen feed gives rise to an increased transport loss with decreasing Pt loading.[33] As seen in Fig. 10, the oxygen concentration on the Pt surface for Pt loading of 0.025 mg/cm^2

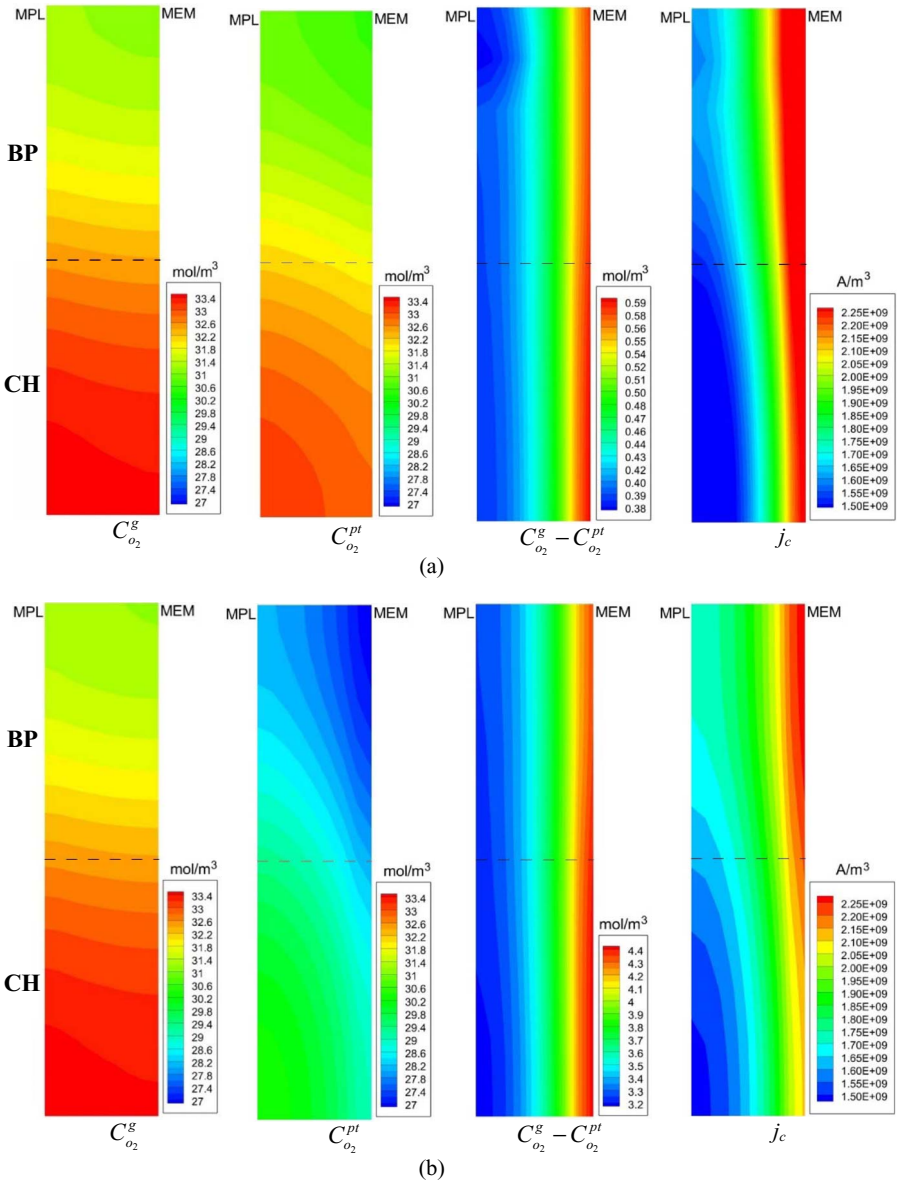

Figure 8. Oxygen concentration in the pore, on the Pt particle surface, concentration drop near the Pt particle and reaction current density distributions in CCL at current density of 2.0 A/cm^2 under pure oxygen, 100% RH, 80 °C and 150 kPa operating condition for Pt loading of 0.2 mg/cm^2 (a) and 0.025 mg/cm^2 (b).

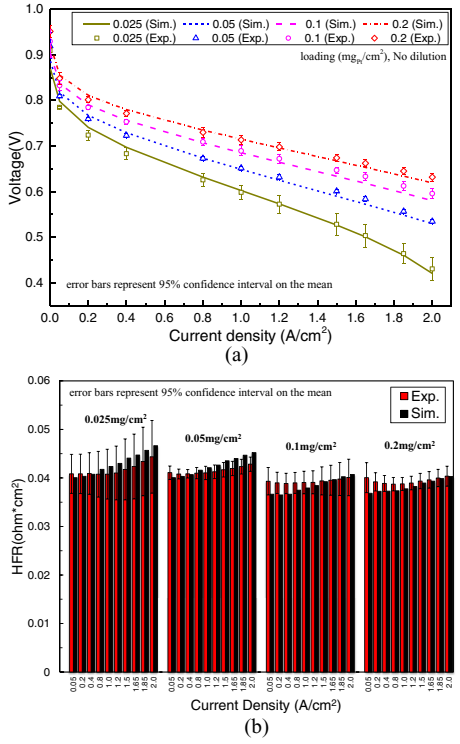

Figure 9. Comparison of polarization curves (a) and HFR (b) between experiments and simulations for non-diluted catalyst under air, 100% RH, 80 °C and 150 kPa operating condition.

is much smaller than that for 0.2 mg/cm^2 loading, although their concentrations in the macro pores are close to each other. The oxygen concentration drop in the cathode catalyst layer is mostly caused by the transport resistance near the Pt particle rather than the macro diffusion resistance through the layer at low Pt loading. This suggests that the cells with low Pt loading still have significant oxygen available in the catalyst layer pores but cannot reach the reaction sites under high current density. In addition, the reaction current density distribution with air and pure oxygen appears different. For pure oxygen, the reaction current density under the rib is a little higher than under the channel due to smaller ionomer conductivity with higher RH there. Under air condition, however, the reaction current density under the channel is higher, especially at the loading of 0.025 mg/cm^2. This difference indicates that the mass transfer begins to dominate in ORR at higher current density for low Pt loading with air feed. On the other hand, the reaction near the catalyst layer/membrane interface cannot further increase once the mass transfer limitation occurs there, although there is higher overpotential. The reaction therefore spreads to the regions with higher oxygen concentration near the MPL/CL interface, as shown in Fig. 10b for low Pt loading case.

The model validation under a drier condition with 65% inlet RH is also performed and the results are plotted in Fig. 11. Again, the predicted results match the measured polarization curves and the HFR values very well. Cells under a drier condition have lower ionomer conductivity and higher electrode resistance because of lower oxygen diffusivity in ionomer, thus leading to higher HFR and worse performance.

With carbon dilution.— The cell polarization curves and HFR for carbon diluted electrode with air feed are shown in Fig. 12 and Fig. 13 for inlet RH of 100% and 65%, respectively. Evidently, the model captures the dilution effect on cell performance and there is

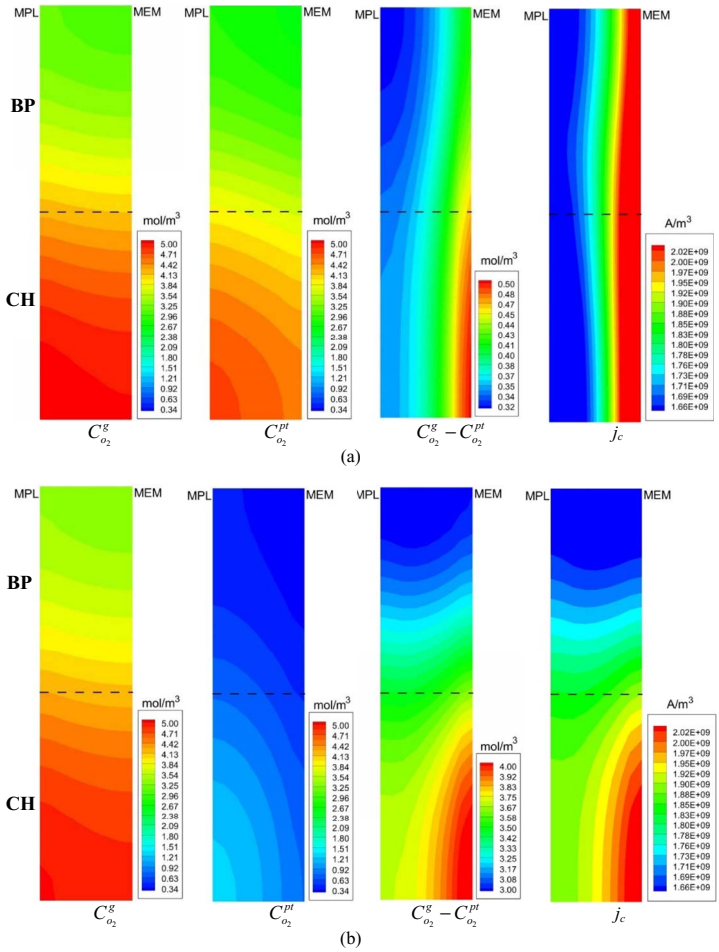

Figure 10. Oxygen concentration in the pore, on the Pt particle surface, concentration drop near the Pt particle and reaction current density distributions in CCL at current density of 2.0 A/cm^2 under air, 100% RH, 80 °C and 150 kPa operating condition for Pt loading of 0.2 mg/cm^2 (a) and 0.025 mg/cm^2 (b).

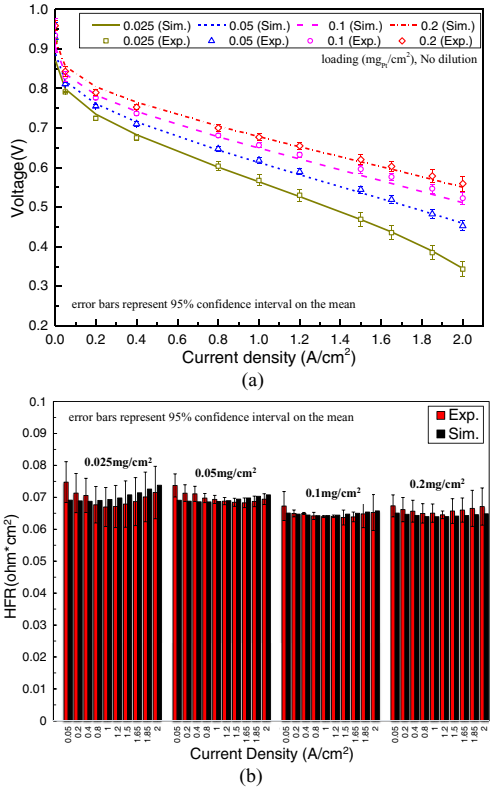

Figure 11. Comparison of polarization curves (a) and HFR (b) between experiments and simulations for non-diluted catalyst under air, 65% RH, 80 °C and 150 kPa operating condition.

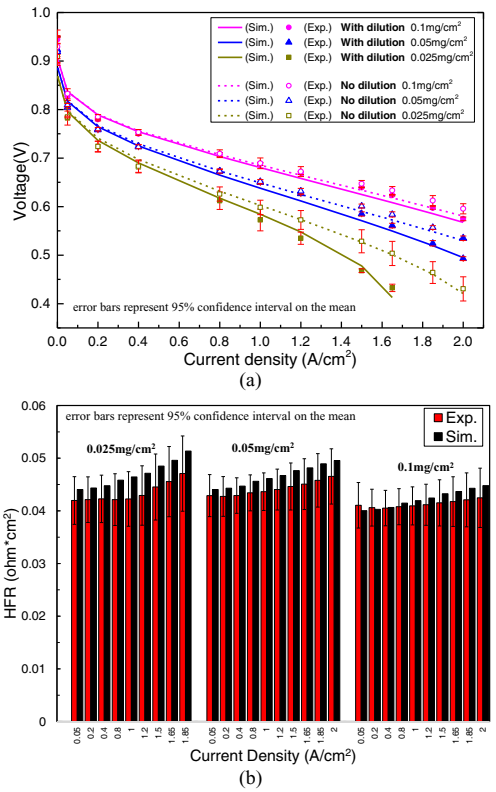

Figure 12. Predicted and measured polarization curves (a) and HFR (b) for carbon diluted catalyst under air, 100% inlet RH, 80 °C and 150 kPa operating condition. Non-diluted polarization curves are also plotted in (a) for comparison.

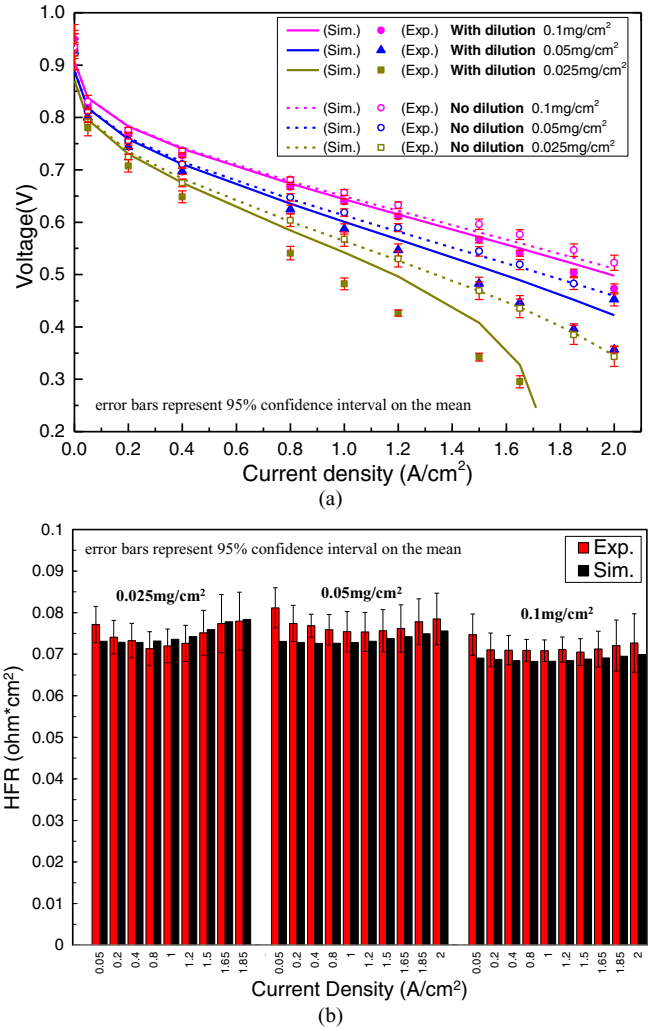

Figure 13. Predicted and measured polarization curves (a) and HFR (b) for carbon diluted catalyst under air, 65% inlet RH, 80 °C and 150 kPa operating condition. Non-diluted polarization curves are also plotted in (a) for comparison.

still good agreement between the predictions and experiments. The mixture of bare carbon into a catalyst layer indeed reduces the cell performance for a given Pt loading. As shown in Fig. 5b, the transport resistance begins to have obvious increase after the number fraction of catalyst particles is lower than 0.25 and dramatically increases if the fraction is lower than 0.1. For case 5 of 0.1 mg/cm^2 loading listed in Table III, the catalyst particles fraction is about 0.265, so the dilution has negligible influence on the cell performance, as shown in Fig. 12 and 13. However, for case 7 of 0.025 mg/cm^2 loading, the catalyst particles fraction is as low as 0.055, and significant performance loss is observed in both RH conditions compared with the non-diluted case. These results indicate the very important role of the electrode composition besides Pt loading.

Agglomeration effect.— In the preceding sections, we have used a homogeneous electrode model based on the recent SEM observations that the agglomerates probably do not exist. However, some literature argued that agglomerates may exist. As mentioned in the introduction, even though the agglomerates exist, their size is not very large. In this section, we will examine whether these small agglomerates have significant impacts on the homogeneous model.

Most of agglomerate models assume ionomer filled agglomerates. However, there is still a debate about this assumption. Actually, because the ionomer has a chain structure with the diameter of 3 to 5

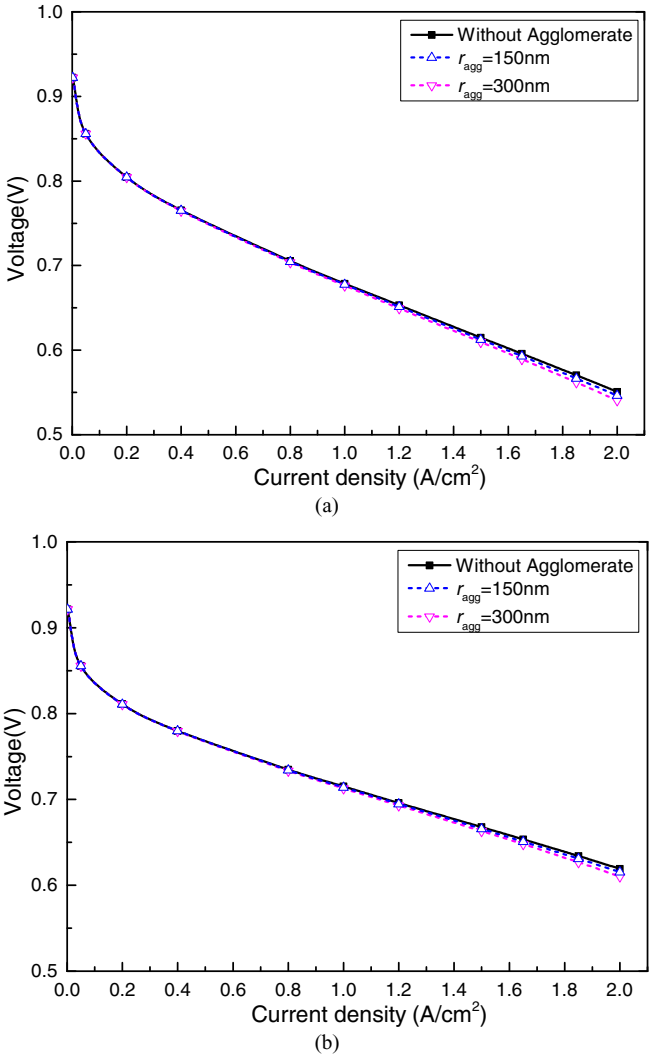

Figure 14. Agglomerate size effect on polarization curve prediction for Pt loading of 0.2 mg/cm^2 at 65% (a) and 100% (b) inlet RH.

nm,[9,22] it cannot easily enter the small pores in the agglomerates. On the other hand, for a common amount of ionomer, for example I/C of 0.95, the ionomer filling all of the agglomerates seems impossible. Therefore, the agglomerates are probably partially filled by ionomer, while some void space remains, as observed by Suzuki et al.[21] We assume the agglomerate including both Pt/C particles and bare carbon particles as the homogeneous electrode. The detailed governing equations of the agglomerate model can be found in Appendix B. Isothermal and isopotential assumptions are used within each agglomerate. These assumptions are valid in a general electrode having heat conductivity higher than 1×10^{-6} W/ (cm K) and ionomer conductivity higher than 1×10^{-4} S/cm.[9,12] Fig. 14 and Fig. 15 shows the agglomerate size effect on the polarization curve prediction for Pt loading of 0.2 mg/cm^2 and 0.025 mg/cm^2, respectively. The ionomer film thickness around the agglomerate is assumed to be 8 nm and the interfacial transport coefficient is the same as the homogeneous model. It can be found that results predicted by the agglomerate model show little difference from the homogenous model prediction for agglomerate radius smaller than 150 nm. The agglomeration effect becomes important after the agglomerate reaching radius larger than 300 nm for the low Pt loading case. However, such a large agglomerate size is not supported by SEM micrographs. For this reason, we believe that the agglomeration effect can be ignored and the foregoing homogeneous electrode

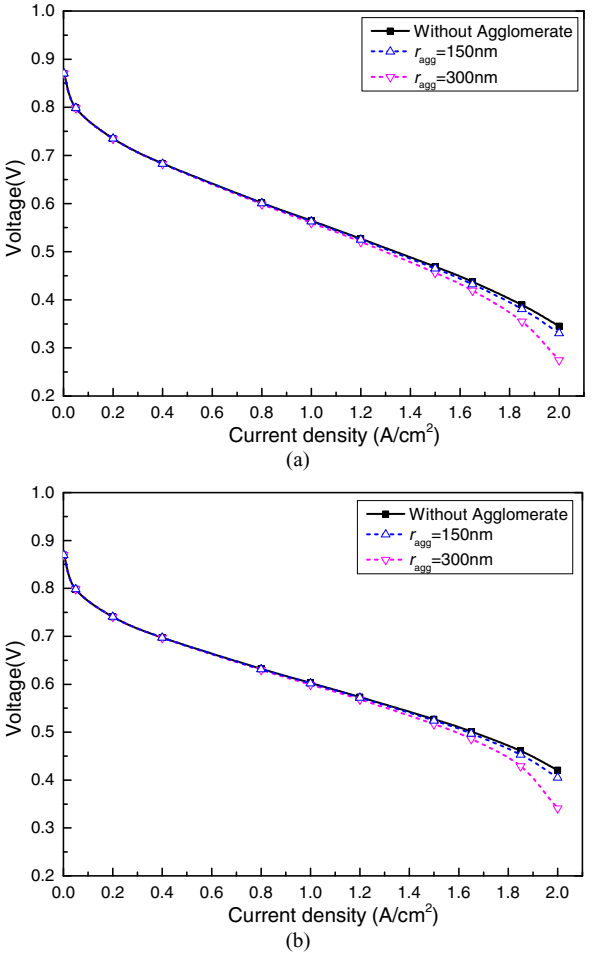

Figure 15. Agglomerate size effect on polarization curve prediction for Pt loading of 0.025 mg/cm^2 at 65% (a) and 100% (b) inlet RH.

model is sufficient to describe the transport and electrochemical phenomena in the PEM fuel cell catalyst layer. We notice that some studies on agglomerate model showed significant effect of agglomerate on cell performance for agglomerate size larger than 100 nm.[23] There are two reasons for this difference. First, we assume that the agglomerates are not filled by ionomer.[21,22] Even if the void pores are filled by water, the effective oxygen diffusivity in water

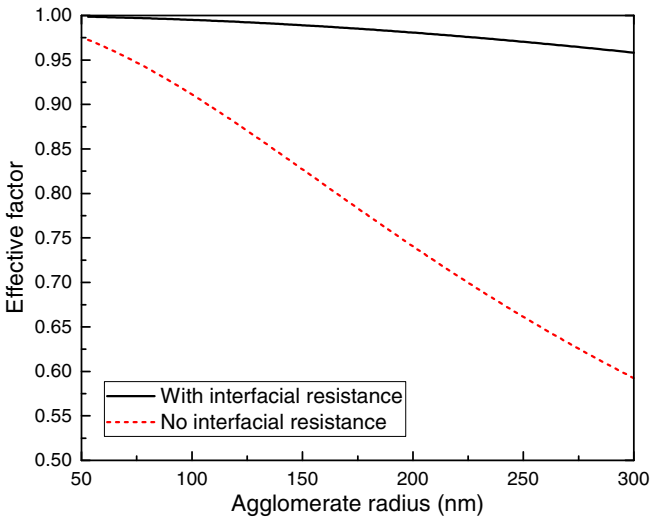

Figure 16. Effective factor with and without the interfacial resistance.

is more than one order of magnitude larger than in ionomer. Second, we introduce the interfacial transport resistances at ionomer film and Pt particle surfaces. These resistances make the oxygen concentration in the agglomerate more uniform, thus a higher effective factor of the agglomerate is obtained. Fig. 16 shows the agglomerate effective factor with and without the interfacial resistances. The presence of the interfacial resistances results in a higher effective factor so that the reaction in the agglomerate is more uniform because the oxygen transport is controlled by the interfacial resistances rather than the diffusion resistance inside the agglomerate.

Conclusions

In this work, a homogeneous electrode model is developed based on the assumption of no agglomerate or sufficiently small agglomerates (<150 nm). By introducing the interfacial transport resistances at ionomer and Pt particle surfaces, Pt loading and catalyst material fraction are taken into consideration in the present electrode model. The electrode transport resistance is found to dramatically increase not only for Pt loading lower than 0.1 mg/cm^2 but also for catalyst material fraction lower than 0.2. We have implemented this electrode model into a full PEM fuel cell model and studied the effect of Pt loading and electrode composition, with and without carbon dilution, on cell performance. The predicted polarization curves and HFR are in very good agreement with the extensive experimental data of Owejan et al.[33] under different operating conditions. The agglomerate is also found to have negligible effect on the cell performance prediction if the agglomerate radius is smaller than 150 nm. For a practical electrode design, this agglomerate size is believed to be the upper limitation, if agglomerates indeed exist in a real catalyst layer, suggesting that the homogeneous electrode assumption is sufficient to predict cell performance.

List of Symbols

A	Area (m^2)
a	Water activity
a_{pt}	Active volumetric surface area of Pt (m^2/m^3)
a_{ECSA}	Electrochemical specific area of Pt (m^2/g$_{pt}$)
a_c	Volumetric surface area of ionomer (m^2/m^3)
C_{o_2}	Oxygen concentration (mol/m^3)
D_{o_2}	Oxygen diffusivity (m^2/s)
E	Cathode potential vs. RHE (V)
E_c	Activation energy in oxygen reduction reaction (J/mol)
F	Faraday's Constant
$H_{o_2,e}$	Henry's constant of oxygen at ionomer surface
I/C	Ionomer to carbon weight ratio
$i_{o,c}$	Exchange current density of oxygen reduction reaction (A/m^2)
j_c	Volumetric current density of oxygen reduction reaction (A/m^3)
k_1	Transport resistance coefficient at ionomer film surface
k_2	Transport resistance coefficient at Pt particle surface
k_3	Transport resistance coefficient at water film surface
L_{pt}	Pt loading (mg/cm^2)
n_c	Number density of carbon particles (/m^3)
n_{pt}	Number of Pt particles on a Pt/C particle
N_{o_2}	Oxygen flux (mol/m^2 s)
R	Ideal-gas constant
$R_{e,int}$	Interfacial transport resistance at ionomer film surface (s/m)
$R_{pt,int}$	Interfacial transport resistance at Pt surface (s/m)
$R_{w,int}$	Interfacial transport resistance at water film surface (s/m)
r_{agg}	Radius of agglomerate (m)
r_c	Radius of carbon particle (m)
r_{pt}	Radius of Pt particle (m)
s	Water saturation
T	Temperature (K)
x	Number fraction of Pt/C particles
wt	Weight percentage (%)

Greek

α_c	Transfer coefficient of oxygen reduction reaction
γ	Reaction order
δ_{CL}	Catalyst layer thickness (m)
ε	Porosity
η_c	Over potential (V)
θ_{PtO}	Pt-oxide coverage
κ	Ionomer proton conductivity (s/m)
λ	Water content in ionomer
ρ	Density (kg/m^3)
τ	Tortuosity
ω	Energy parameter for Temkin isotherm (J/mol)

Subscripts

a	Anode
c	Carbon; cathode
CL	Catalyst layer
e	Ionomer
int	Interface
w	Water

Superscripts

agg	Agglomerate
eff	Effective value
g	Gas
pt	Platinum
ref	Reference value

Appendix A

Catalyst layers may have several types of Pt/C materials with different Pt weight percentage. Here, we consider a blended catalyst layer with two catalyst types, and with bare carbon as the diluent. For simplification, number 1 and 2 indicate catalyst material 1 and 2, respectively, and number 0 indicates the bare carbon. Assuming the carbon support of the catalyst has the same size as the bare carbon, we can obtain the volume fraction (or number fraction) of catalyst type1 x_1, type2 x_2 and bare carbon x_0 as follows,

$$x_1 = \frac{(1 - wt_1\%)y_1}{(1 - wt_1\%)y_1 + (1 - wt_2\%)y_2 + y_0} \quad [A1]$$

$$x_2 = \frac{(1 - wt_2\%)y_2}{(1 - wt_1\%)y_1 + (1 - wt_2\%)y_2 + y_0} \quad [A2]$$

$$x_0 = \frac{y_0}{(1 - wt_1\%)y_1 + (1 - wt_2\%)y_2 + y_0} \quad [A3]$$

where y_1, y_2 and y_0 are the weight fraction of the catalyst type 1, 2 and bare carbon, respectively.

The contribution of the current density for each catalyst type depends on its Pt particle number density, so we have,

$$j_1 + j_2 = j_c \quad [A4]$$

$$\frac{j_1}{j_2} = \frac{n_{pt1}x_1}{n_{pt2}x_2} \quad [A5]$$

where j_1 and j_2 are the volume current density for catalyst type 1 and 2, respectively. j_c is the total volume current density. n_{pt} is the Pt particle number on a Pt/C particle, which is given by Equation 19. From A4 and A5, j_1 and j_2 can be obtained by,

$$j_1 = \frac{n_{pt1}x_1}{n_{pt1}x_1 + n_{pt2}x_2} j_c \quad [A6]$$

$$j_2 = \frac{n_{pt2}x_2}{n_{pt1}x_1 + n_{pt2}x_2} j_c \quad [A7]$$

From Equation 29, the oxygen concentration difference between $C^g_{o_2}$ and $C^{pt}_{o_2}$ for catalyst type1 and 2 are,

$$\Delta C_{o_2,1} = -\left[(k_3 + 1)\frac{\delta_w}{D_{o_2,w}} + \left(k_1 + \frac{(r_c + \delta_e)^2}{r_{pt}^2(1 - \theta_{PtO})}\frac{\rho_{pt}}{\rho_c}\left(\frac{r_{pt}}{r_c}\right)^3 \times \left(\frac{1 - wt_1\%}{wt_1\%}\right)(k_2 + 1)\right)\frac{\delta_e}{D_{o_2,ion}}\right]\frac{j_1}{4Fa_cx_1} \quad [A8]$$

$$\Delta C_{o_2,2} = -\left[(k_3+1)\frac{\delta_w}{D_{o_2,w}} + \left(k_1 + \frac{(r_c+\delta_e)^2}{r_{pt}^2(1-\theta_{PtO})}\frac{\rho_{pt}}{\rho_c}\left(\frac{r_{pt}}{r_c}\right)^3 \times \left(\frac{1-wt_2\%}{wt_2\%}\right)(k_2+1)\right)\frac{\delta_e}{D_{o_2,ion}}\right]\frac{j_2}{4Fa_cx_2} \quad [A9]$$

The average oxygen concentration difference is assumed as,

$$\Delta C_{o_2,\text{avg}} = \Delta C_{o_2,1}\frac{x_1}{x_1+x_2} + \Delta C_{o_2,2}\frac{x_2}{x_1+x_2} \quad [A10]$$

Equation A10 defines the average oxygen concentration difference by a volume averaged method. Substitute A6–A9 and Equation 19 into A10, we get,

$$\Delta C_{o_2,avg} = -\left[(k_3+1)\frac{\delta_w}{D_{o_2,w}} + \left(k_1 + \frac{(r_c+\delta_e)^2}{r_{pt}^2(1-\theta_{PtO})}\frac{\rho_{pt}}{\rho_c}\left(\frac{r_{pt}}{r_c}\right)^3 \times \left(\frac{x_1+x_2}{x_1\frac{wt_1\%}{1-wt_1\%}+x_2\frac{wt_2\%}{1-wt_2\%}}\right)(k_2+1)\right)\frac{\delta_e}{D_{o_2,ion}}\right]\frac{j_c}{4Fa_c(x_1+x_2)} \quad [A11]$$

If we define the average Pt weight percentage of the mixed catalyst material by,

$$wt_{avg}\% = \frac{y_1wt_1\% + y_2wt_2\%}{y_1+y_2} \quad [A12]$$

From Equation A12 and A1–A2, one has,

$$\frac{wt_{avg}\%}{1-wt_{avg}\%} = \frac{x_1}{x_1+x_2}\frac{wt_1\%}{1-wt_1\%} + \frac{x_2}{x_1+x_2}\frac{wt_2\%}{1-wt_2\%} \quad [A13]$$

Finally, Equation A11 becomes,

$$\Delta C_{o_2,avg} = -\left[(k_3+1)\frac{\delta_w}{D_{o_2,w}} + \left(k_1 + \frac{(r_c+\delta_e)^2}{r_{pt}^2(1-\theta_{PtO})}\frac{\rho_{pt}}{\rho_c}\left(\frac{r_{pt}}{r_c}\right)^3 \times \left(\frac{1-wt_{avg}\%}{wt_{avg}\%}\right)(k_2+1)\right)\frac{\delta_e}{D_{o_2,ion}}\right]\frac{j_c}{4Fa_c(x_1+x_2)} \quad [A14]$$

and the total transport resistance near the Pt/C particles is expressed as,

$$R_T = \left[(k_3+1)\frac{\delta_w}{D_{o_2,w}}\frac{a_{ECSA}}{a_cf_t} + \left(k_1\frac{a_{ECSA}}{a_cf_t} + \frac{k_2+1}{1-\theta_{PtO}}\left(\frac{1-wt_{vg}\%}{wt_{vg}\%}\right)\right)\frac{\delta_e}{D_{o_2,ion}}\right]\frac{f_t}{a_{ECSA}\delta_{CL}}\frac{1}{x} \quad [A15]$$

Equation A15 is the same as Equation 30 when using the average Pt weight percentage A12. Although Equation A15 is derived from two types of catalyst, it can be used for any mixed catalyst formulation if the carbon support has the same size, where the average Pt weight percentage and total number fraction of the Pt/C particles are given by,

$$wt_{avg}\% = \frac{\sum_N y_iwt_i\%}{\sum_N y_i} \quad [A16]$$

$$x = \frac{\sum_N y_i(1-wt_i\%)}{\sum_N y_i(1-wt_i\%) + y_{\text{bare}}} \quad [A17]$$

where N is the number of the catalyst type and y_{bare} is the bare carbon weight parentage. Using A16, A17 is reduced to,

$$x = \frac{(1-wt_{avg}\%)(1-y_{bare})}{1-wt_{avg}\%(1-y_{bare})} \quad [A18]$$

Additionally, the total Pt loading in the catalyst layer of the mixed catalysts is,

$$L_{pt} = \sum x_i\cdot n_c\cdot\delta_{CL}\cdot n_{pt,i}\cdot\frac{4}{3}\pi r_{pt}^3\cdot\rho_{pt} = \sum x_i\frac{\delta_{CL}}{f_t}\frac{wt_i\%}{1-wt_i\%} \quad [A19]$$

Using A16 and A17, Equation A19 can be rewritten by,

$$L_{pt} = x\frac{\delta_{CL}}{f_t}\frac{wt_{avg}\%}{1-wt_{avg}\%} \quad [A20]$$

As a result, Equation A15 becomes Equation 32.

Appendix B

Consider an agglomerate shown in Fig. B1. The agglomerate may include both Pt/C particles and bare carbon particles. In addition, the agglomerate is probably not filled by the ionomer, as discussed in the main text. Assuming that the electronic and ionomer potentials in the agglomerate are constant, the diffusion equation of oxygen in the agglomerate is described by:

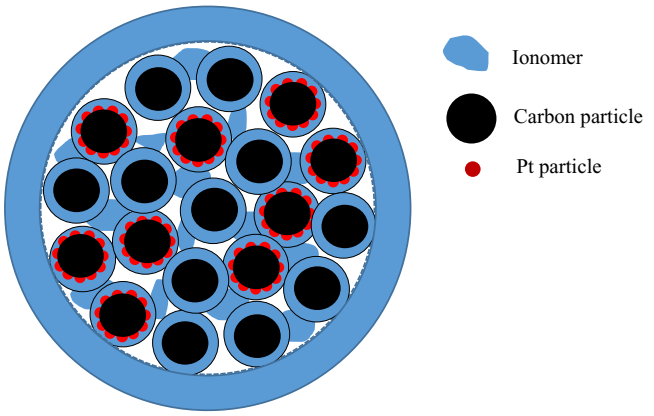

Figure B1. Illustration of an agglomerate.

$$\frac{1}{r^2}\frac{d}{dr}\left(r^2D_e^{agg}\frac{dC_{o2}}{dr}\right) + j_{o2} = 0 \quad [B1]$$

where

$$j_{o_2} = \frac{j_c}{4F} = -\frac{1}{4F}i_{0,c}a_{pt}(1-\theta_{POH})\left(\frac{C_{O2}^{pt}}{C_{O_2,ref}}\right)^\gamma\exp\left(-\frac{a_c}{RT}F\eta_c - \frac{\omega\theta_{POH}}{RT}\right) \quad [B2]$$

If we use $D = i_{0,c}a_{pt}(1-\theta_{POH})(\frac{1}{C_{O_2,ref}})^\gamma\exp(-\frac{a_c}{RT}F\eta_c - \frac{\omega\theta_{POH}}{RT})$ Equation B2 is reduced to be,

$$j_{o_2} = -\frac{D}{4F}(C_{O2}^{pt})^\gamma \quad [B3]$$

For each Pt/C particle in the agglomerate, the relationship between the O_2 concentration near the Pt particles $C_{o_2}^{pt}$ and the O_2 concentration in the pores of the agglomerate C_{o_2} is given by Equation 18, which is,

$$D\left(C_{o_2}^{pt}\right)^\gamma + \frac{4F}{A/(a_cx)}C_{o_2}^{pt} - \frac{4F}{A/(a_cx)}C_{o_2} = 0 \quad [B4]$$

From B4, the O_2 concentration near Pt particle can be solved. For a general case, the oxygen reduction flux B3 can be expressed as a function of C_{o_2} instead of $C_{o_2}^{pt}$, which is,

$$j_{o_2} = -f(A,D)D(C_{O_2})^\gamma \quad [B5]$$

where $f(A,D)$ is a function solved from B4. If ignoring the interfacial transport resistances inside the agglomerate, $f(A,D) = 1$. Using the effectiveness-factor method to indicate the agglomerate effect on O_2 transfer phenomena and kinetics, the analytic solution of the effective factor can be obtained for first-order reaction,

$$E_r = \frac{3}{\xi^2}(\xi\coth\xi - 1) \quad [B6]$$

where ξ is the Thiele modulus. Though B6 is from the first-order reaction, it also can be used in non-first order reaction[12] if the Thiele modulus uses the following expression,

$$\xi = r_{agg}\sqrt{\frac{f\cdot D\cdot(C_{o_2,s})^{\gamma-1}}{4F\cdot D_{eff}^{agg}}} \quad [B7]$$

where r_{agg} is the radius of the agglomerate, D_{eff}^{agg} is the effective diffusivity of O_2 in the agglomerate, $C_{o_2,s}$ is the O_2 concentration on the agglomerate surface.

If the agglomerate is covered by ionomer or liquid water, the oxygen reduction flux satisfies the following equation,

$$-\frac{4F\cdot j_{o_2}}{E_r\cdot f\cdot D} = \left(C_{o_2}^g + \frac{j_{o_2}R_{agg,\text{int}}}{a_{agg}}\right)^\gamma \quad [B8]$$

where $R_{\text{agg,int}}$ is the transport resistance through the ionomer or water film covering the agglomerate, which includes the interfacial resistance and bulk film transport resistance; a_{agg} is the agglomerate surface area per volume. For first order reaction where $\gamma = 1$, the solution of Equation B8 gives,

$$j_{o_2} = -C_{o_2}^g\left[\frac{4F}{E_r\cdot f\cdot D} + \frac{R_{agg,\text{int}}}{a_{agg}}\right]^{-1} \quad [B9]$$

For reaction order different from the unity, a numerical method is used.

References

1. The US Department of Energy (DOE). *Energy Efficiency and Renewable Energy, Multi-Year Research, Development and Demonstration Plan* http://energy.gov/sites/prod/files/2014/03/f12/fuel_cells.pdf.
2. Mark K. Debe, Electrocatalyst Approaches and Challenges for Automotive Fuel Cells, *Nature*, **486**, 43 (2012).
3. Mark K. Debe, Effect of Electrode Surface Area Distribution on High Current Density Performance of PEM Fuel Cells, *Journal of The Electrochemical Society*, **159**, B53 (2012).
4. Mark K. Debe, Nanostructured Thin Film Electrocatalysts for PEM Fuel Cells – A Tutorial on the Fundamental Characteristics and Practical Properties of NSTF Catalysts, *ECS Transactions*, **45**, 47 (2012).
5. Daniel R. Baker, David A. Caulk, Kenneth C. Neyerlin, and Michael W. Murphy, Measurement of Oxygen Transport Resistance in PEM Fuel Cells by Limiting Current Methods, *Journal of The Electrochemical Society*, **156**, B991 (2009).
6. Nobuaki Nonoyama, Shinobu Okazaki, Adam Z. Weber, Yoshihiro Ikogi, and Toshihiko Yoshida, Analysis of Oxygen-Transport Diffusion Resistance in Proto-Exchange-Membrane Fuel Cells, *Journal of The Electrochemical Society*, **158**, B416 (2011).
7. Tatyana V. Reshetenko and Jean St-Pierre, Separation Method for Oxygen Mass Transport Coefficient in Gas and Ionomer Phases in PEMFC GDE, *Journal of The Electrochemical Society*, **161**, F1089 (2014).
8. Thomas A. Greszler, David Caulk, and Puneet Sinha, The Impact of Platinum Loading on Oxygen Transport Resistance, *Journal of The Electrochemical Society*, **159**, F831 (2012).
9. A. Z. Weber, R. L. Borup, R. M. Darling, P. K. Das, T. J. Dursch, W. Gu, D. Harvey, A. Kusoglu, S. Litster, M. M. Mench, R. Mukundan, J. P. Owejan, J. G. Pharoah, M. Secanell, and I. V. Zenyuk, A Critical Review of Modeling Transport Phenomena in Polymer-Electrolyte Fuel Cells, *Journal of The Electrochemical Society*, **161**, F1254 (2014).
10. Yoshitaka Ono, Tetsuya Mashio, Satoshi Takaichi, Atsushi Ohma, Hiroyuki Kanesaka, and Kazuhiko Shinohara, The Analysis of Performance Loss with Low Platinum Loaded Cathode Catalyst Layers, *ECS Transactions*, **28**, 69 (2010).
11. Yosuke Fukuyama, Takeshi Shiomi, Toshikazu Kotaka, and Yuichiro Tabuchi, The Impact of Platinum Reduction on Oxygen Transport in Proton Exchange Membrane Fuel Cells, *Electrochimica Acta* **117**, 367 (2014).
12. Wonseok Yoon and Adam Z. Weber, Modeling Low-Platinum-Loading Effects in Fuel Cell Catalyst Layers, *Journal of The Electrochemical Society*, **158**, B1007 (2011).
13. S. H. Chan and W. A. Tun, Catalyst Layer Models for Proton Exchange Membrane Fuel Cells, *Chemical Engineering Technology*, **24**, 51 (2001).
14. Datong Song, Qianpu Wang, Zhongsheng Liua, Titichai Navessin, and Steven Holdcroft, Numerical study of PEM fuel cell cathode with non-uniform catalyst layer, *Electrochimica Acta*, **50**, 731 (2004).
15. R. Madhusudana Rao and R. Rengaswamy, Dynamic characteristics of spherical agglomerate for study of cathode catalyst layers in proton exchange membrane fuel cells (PEMFC), *Journal of Power Sources*, **158**, 110 (2006).
16. A. A. Shah, G. S. Kim, W. Gervais, A. Young, K. Promislow, J. Li, and S. Ye, The effects of water and microstructure on the performance of polymer electrolyte fuel cells, *Journal of Power Sources*, **160**, 1251 (2006).
17. M. Eikerling, Water Management in Cathode Catalyst Layers of PEM Fuel Cells-A Structure-Based Model, *Journal of The Electrochemical Society*, **153**, E58 (2006).
18. P. Jain, L. T. Biegler, and M. S. Jhon, Optimization of Polymer Electrolyte Fuel Cell Cathodes, *Electrochemical and Solid-State Letters*, **11**, B193 (2008).
19. Salih Obut and Erdogan Alper, Numerical assessment of dependence of polymer electrolyte membrane fuel cell performance on cathode catalyst layer parameters, *Journal of Power Sources*, **196**, 1920 (2011).
20. J. Marquis and M. O. Coppens, Achieving Ultra-high Platinum Utilization via Optimization of PEM Fuel Cell Cathode Catalyst layer Microstructure, *Chemical Engineering Science*, **102**, 151 (2013).
21. Takahisa Suzuki, Kenji Kudo, and Yu Morimoto, Model for Investigation of Oxygen Transport Limitation in a Polymer Electrolyte Fuel Cell, *Journal of Power Sources*, **222**, 379 (2013).
22. Steven Holdcroft, Fuel Cell Catalyst Layers: A Polymer Science Perspective, *Chemistry of Materials*, **26**, 381 (2014).
23. William K. Epting and Shawn Litster, Effects of an Agglomerate Size Distribution on the PEFC Agglomerate Model, *International Journal of Hydrogen Energy*, **37**, 8505 (2012).
24. Yoshitaka Ono, Atsushi Ohma, Kazuhiko Shinohara, and Kazuyoshi Fushinobu, Influence of Equivalent Weight of Ionomer on Local Oxygen Transport Resistance in Cathode Catalyst Layers, *Journal of The Electrochemical Society*, **160**, F779 (2013).
25. H. Iden, K. Sato, A. Ohma, and K. Shinohara, Relationship among Microstructure, Ionomer Property and Proton Transport in Pseudo Catalyst Layers, *Journal of the Electrochemical Society*, **158**, B987 (2011).
26. T. Soboleva, K. Malek, Z. Xie, T. Navessin, and S. Holdcroft, PEMFC catalyst layers: the role of micropores and mesopores on water sorption and fuel cell activity, *ACS Appl Mater Interfaces*, **3**, 1827 (2011).
27. Miguel A. Modestino, Devproshad K. Paul, Shudipto Dishari, Stephanie A. Petrina, Frances I. Allen, Michael A. Hickner, Kunal Karan, Rachel A. Segalman, and Adam Z. Weber, Self-Assembly and Transport Limitations in Confined Nafion Films, *Macromolecules*, **46**, 867 (2013).
28. R. Makharia, M. F. Mathias, and D. R. Baker, Measurement of Catalyst Layer Electrolyte Resistance in PEFCs Using Electrochemical Impedance Spectroscopy, *Journal of The Electrochemical Society*, **152**, A970 (2005).
29. K. C. Hess, W. K. Epting, and S. Litster, Spatially Resolved, In Situ Potential Measurements through Porous Electrodes As Applied to Fuel Cells, *Analytical Chemistry*, **83**, 9492 (2011).
30. K. Kudo, T. Suzuki, and Y. Morimoto, Analysis of Oxygen Dissolution Rate from Gas Phase into Nafion Surface and Development of an Agglomerate Model, *ECS Transactions*, **33**, 1495 (2010).
31. K. Kudo and Y. Morimoto, Analysis of Oxygen Transport Resistance of Nafion thin film on Pt electrode, *ECS Transactions*, **50**, 1487 (2012).
32. M. Moore, P. Wardlaw, P. Dobson, J. J. Boisvert, A. Putz, R. J. Spiteri, and M. Secanell, Understanding the Effect of Kinetic and Mass Transport Processes in Cathode Agglomerates, *Journal of The Electrochemical Society*, **161**, E3125 (2014).
33. Jon P. Owejan, Jeanette E. Owejan, and Wenbin Gu, Impact of Platinum and Catalyst Layer Structure on PEMFC Performance, *Journal of The Electrochemical Society*, **160**, F824 (2013).
34. Shinji Jomori Kaori Komatsubara, Nobuaki Nonoyama, Manabu Kato, and Toshihiko Yoshida, An Experimental Study of the Effects of Operational History on Activity Changes in a PEMFC, *Journal of The Electrochemical Society*, **160**, F1067 (2013).
35. N. P. Subramanian, T. A. Greszler, J. Zhang, W. Gu, and R. Makharia, Pt-Oxide Coverage- Dependent Oxygen Reduction Reaction (ORR) Kinetics, *Journal of The Electrochemical Society*, **159**, B531 (2012).
36. Yuxiu Liu, Michael W. Murphy, Daniel R. Baker, Wenbin Gu, Chunxin Ji, Jacob Jorne, and Hubert A. Gasteiger, Proton Conduction and Oxygen Reduction Kinetics in PEM Fuel Cell Cathodes: Effects of Ionomer-to-Carbon Ratio and Relative Humidity, *Journal of The Electrochemical Society*, **156**, B970 (2009).
37. Y. Wang, C. Y. Wang, and A Nonisothermal, Two-Phase Model for Polymer Electrolyte Fuel Cells, *Journal of The Electrochemical Society*,**153**, A1193 (2006).
38. K. C. Neyerlin, Wenbin Gu, Jacob Jorne, and Hubert A. Gasteiger, Study of the Exchange Current density for the Hydrogen Oxidation and Evolution Reactions, *Journal of The Electrochemical Society*, **154**, B631 (2007).
39. C. K. Mittelsteadt and H. Liu, "Conductivity, permeability, and ohmic shorting of ionomeric membranes," Chapter 23 of Handbook of Fuel Cells, Vol. 5, W. Vielstich, H. Yokokawa, and H. A. Gasteiger, eds., John Wiley & Sons, 2009
40. D. A. Caulk, A. M. Brenner, and S. M. Clapham, A Steady Permeation Method for Measuring Water Transport Properties of Fuel Cell Membranes, *Journal of The Electrochemical Society*, **159**, F518 (2012).